A pyrene-inhibitor fluorescent probe with large Stokes shift for the staining of $A\beta_{1-42}$, α-synuclein and amylin amyloid fibrils as well as amyloid-containing *Staphylococcus aureus* biofilms

Alejandro Mahía,[1,2] María Conde-Giménez,[1,2] Sandra Salillas,[1,2] Irantzu Pallares,[5] Juan J. Galano[1,2], Íñigo Lasa,[4] Salvador Ventura,[5] María D. Díaz-de-Villegas,[6] José A. Gálvez,[6] and Javier Sancho*[1,2,3]

[1]Departamento de Bioquímica y Biología Molecular y Celular, Facultad de Ciencias, Universidad de Zaragoza, Pedro Cerbuna 12, 50009 Zaragoza, Spain

[2]Biocomputation and Complex Systems Physics Institute (BIFI). Joint Unit IQFR-CSIC-BIFI, Joint Unit EEAD-CSIC-BIFI, Mariano Esquillor s/n, Edificio I+D, Zaragoza, Spain

[3]Aragon Health Research Institute (IIS Aragón), University of Zaragoza, Zaragoza, Spain

[4]Navarrabiomed, Universidad Pública de Navarra-Departamento de Salud, Pamplona-31008, Navarra, Spain

[5]Institut de Biotecnologia i de Biomedicina and Departament de Bioquímica i Biologia Molecular. Universitat Autònoma de Barcelona. E-08193 Bellaterra, Spain

[6]Instituto de Síntesis Química y Catálisis Homogénea (ISQCH), CSIC–Universidad de Zaragoza, Departamento de Química Orgánica, Pedro Cerbuna 12, 50009 Zaragoza, Spain

*Correspondence to: jsancho@unizar.es

ACKNOWLEDGMENTS

IL is supported by the Spanish Ministry of Economy and Competitiveness grant BIO2014-53530-R. SV is supported by Grant BIO2016-783-78310-R and by ICREA, ICREA-Academia 2015. MDD is supported by Government of Aragon (GA E-102). JS is supported by grants BFU2016-78232-P (MINECO, Spain) and E45_17R (Gobierno de Aragón, Spain). JS and IL acknowledge financial support from grant CI-2017/001-3 (Campus Iberus, Spain). A.M. was recipient of a predoctoral FPU fellowship from the Spanish Government. Authors would like to acknowledge the use of Servicio General de Apoyo a la Investigación-SAI, Universidad de Zaragoza. We thank Dr. N. Cremades for her generous gift of α-syn and Dr. V. Fernández-Moreira and Prof. M. C. Gimeno for the measurement of lifetime and quantum yield values.

ABSTRACT

Amyloid fibrils formed by a variety of peptides are biological markers of different human diseases, such as Alzheimer, Parkinson or Type II diabetes, and are structural constituents of bacterial biofilms. Novel fluorescent probes offering improved sensitivity or specificity towards that diversity of amyloid fibrils, or providing alternative spectral windows are needed to improve the detection or the identification of amyloid structures. One potential source for such new probes is offered by molecules known to interact with fibrils, such as the inhibitors of amyloid aggregation found in drug discovery projects. Here, we show the feasibility of the approach by designing, synthesizing and testing several pyrene-based fluorescent derivatives of a previously discovered inhibitor of the aggregation of the $A\beta_{1-42}$ peptide. All the derivatives tested retain the interaction with the amyloid architecture and allow its staining. The more soluble derivative, compound 1D, stains similarly well amyloid fibrils formed by $A\beta_{1-42}$, α-synuclein or amylin, provides a sensitivity only slightly lower than that of Thioflavin T, displays a large Stokes shift, allows an efficient excitation in the UV spectral region, and it is not cytotoxic. Compound 1D can also stain amyloid fibrils formed by Staphylococcal peptides present in biofilm matrices and can be used to distinguish, by direct staining, *S. aureus* biofilms containing amyloid forming phenol soluble modulins from those lacking them.

Keywords: amyloid fibrils, aggregation inhibitor, pyrene, Stokes shift, fluorescent probes, biofilm matrix

GRAPHICAL ABSTRACT

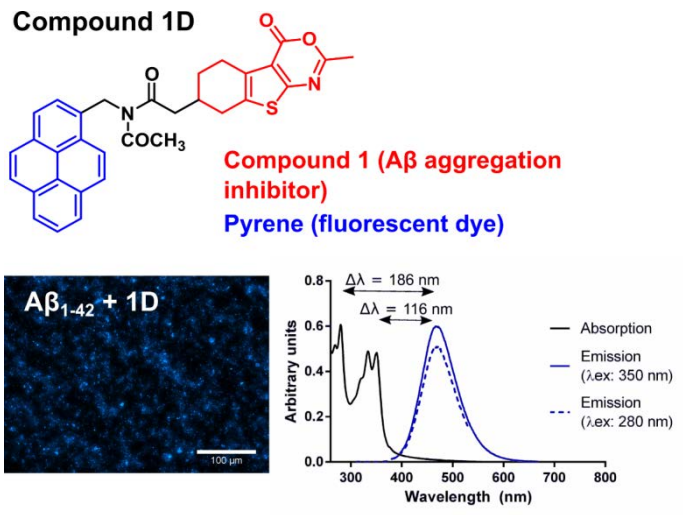

INTRODUCTION

More than 46 million people are affected by Alzheimer's disease (AD) [1–3], a neurodegenerative disorder that, since its discovery in 1906 [4], has become the major cause of dementia in humans. Because getting older is the main risk factor for the development of AD [5–7] and average life expectancy keeps rising, there is a need to develop effective therapeutic drugs and diagnostic tools targeting the main biomarkers of the disease. The two classic lesions that characterize AD are senile plaques made of extracellular fibrillar deposits of amyloid beta peptide (Aβ) aggregates, and intraneuronal neurofibrillary tangles composed of hyperphosphorylated tau protein [8]. The main components of amyloid plaques are two N-terminal β-amyloid precursor protein (APP) fragments [9–11]: $A\beta_{1\text{-}40}$ and $A\beta_{1\text{-}42}$, the latter having the greatest aggregating activity due to its lower solubility.

According to the amyloid cascade hypothesis, aggregation of Aβ peptide triggers the development of AD [12]. Blocking the Aβ production/aggregation cascade seems a promising strategy to develop drugs for AD treatment [13]. By adapting high throughput experimental screening methods previously used to discover pharmacological chaperones [14] and protein inhibitors [15], we reported the discovery of four compounds that inhibit the aggregation of $A\beta_{17\text{-}40}$ and $A\beta_{1\text{-}42}$ both *in vitro* and in fungi models [16]. As those compounds interact with Aβ aggregating species [17] suitable fluorescent derivatives could be used to detect and quantitate Aβ fibrils by means of fluorescence microscopy. Thioflavin T (ThT) is at present the fluorescent probe most commonly used to stain amyloid fibrils and to follow the aggregation kinetics of amyloidogenic proteins [18]. ThT recognizes the generic amyloid motif and interacts with the fibrils formed by diverse, unrelated proteins [19]. New fluorescent probes with increased sensitivity or selectivity, or that allow broadening the working spectroscopic window could help improve the detection or the identification of amyloid structures.

In amyloidogenic diseases, amyloid fibril formation occurs upon aberrant misfolding of soluble, functional proteins. However, amyloid fibrils are not always the result of aberrant protein folding, and some are produced on purpose under non-pathological conditions. Thus, the microbial world makes use of this type of protein fibrils for a number of processes, such as adhesion to host tissues [20] and the building of structural scaffolds in biofilm matrices [21]. One of the first examples of amyloid systems related to biofilm matrix formation was described in *Staphylococcus aureus*. Functional fibrils with amyloidogenic properties formed by the polymerization of small peptides known as phenol-soluble modulins (PSMs) increase the stability of *S. aureus* biofilms [22]. A fluorescent chemical compound that could stain amyloid-like structures would be useful to detect the amyloid nature of the bacterial biofilm matrix formed by pathogenic bacteria.

Our aim is to develop new fluorescent markers for the detection of Aβ and other amyloid fibrils by attaching a high quantum yield fluorescent dye to an organic

molecular scaffold that has been previously demonstrated to interact with Aβ aggregates. Herein, we report the design, synthesis, and *in vitro* testing of several fluorescent derivatives of compound 1 (Chart 1). One of them, compound 1D, stains Aβ, amylin and α-synuclein fibrils and is shown to specifically label PSMs amyloidogenic fibrils in the *S. aureus* biofilm matrix.

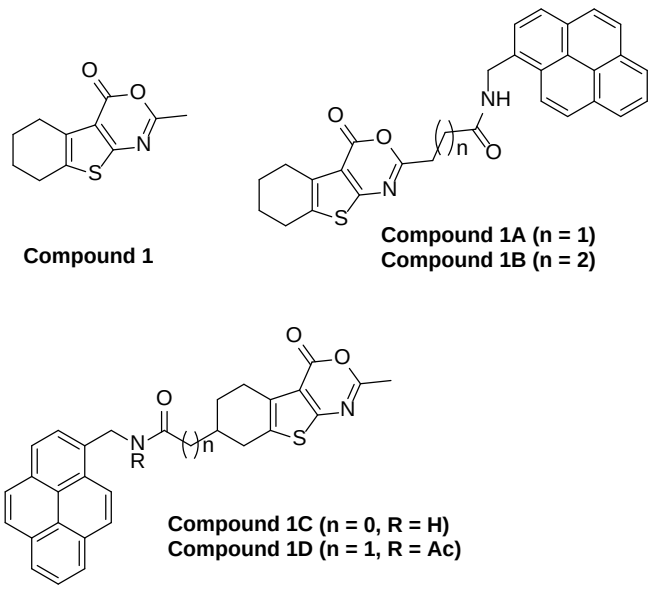

Chart 1. Chemical structures of Compound 1 and its fluorescent derivatives

MATERIALS AND METHODS

Chemicals, peptides and proteins

All chemicals for synthesis were obtained from commercial suppliers and were used without further purification. $A\beta_{17-40}$ and Ac-amylin 8-37 were purchased from GeneCust, $A\beta_{1-42}$ from GenicBio, and α-PSM1 and α-PSM4 from ChinaPeptides. Alpha-synuclein fibrils (171 μM in PBS buffer) were a generous gift from Dr. NC. A $A\beta_{17-40}$ stock solution (418 μM) was prepared by dissolving lyophilized peptide in 5 % formic acid and was stored at -80 ºC. Stock solutions (2 mM) of $A\beta_{1-42}$ and Ac-amylin 8-37 in DMSO were prepared as follows. Peptide was dissolved (1 mg/mL) in hexafluoro-2-propanol (HFIP), placed in a bath sonicator for 5 min, and incubated at room temperature for 2 hours. Then, HFIP was evaporated by a flow of N_2, and dry peptide was dissolved in DMSO and stored at -80 ºC. A 0.3 mM stock solution of BSA (Sigma-Aldrich) was prepared in PBS buffer (10 mM NaH_2PO_4, 150 mM NaCl and pH 7). ThT was purchased from Sigma-Aldrich, and a 650 μM stock solution was prepared in PBS buffer.

Synthesis and instrumentation for products characterization

Synthetic procedures, characterization and ^{1}H-NMR and ^{13}C-NMR spectra are reported in the Electronic Supplementary Material (ESM). Stock solutions (4 mM) in DMSO were prepared for the studied compounds: 3-(4-Oxo-5,6,7,8-tetrahydro-4*H*-benzo[4,5]thieno[2,3-*d*][1,3]oxazin-2-yl)-*N*-(pyren-1-ylmethyl)propanamide (compound 1A), 4-(4-Oxo-5,6,7,8-tetrahydro-4*H*-benzo[4,5]thieno[2,3-*d*][1,3]oxazin-2-yl)-*N*-(pyren-1-ylmethyl)butanamide (compound 1B), 2-Methyl-4-oxo-*N*-(pyren-1-ylmethyl)-5,6,7,8-tetrahydro-4*H*-benzo[4,5]thieno[2,3-*d*][1,3]oxazine-7-carboxamide (compound 1C) and *N*-Acetyl-2-(2-methyl-4-oxo-5,6,7,8-tetrahydro-4*H*-benzo[4,5]thieno[2,3-*d*][1,3]oxazin-7-yl)-*N*-(pyren-1-ylmethyl)acetamide (compound 1D). Melting points were determined in open glass capillaries on a Gallenkamp apparatus. Infrared spectra were registered on a Fourier Transform-Infrared spectrometer (Nicolet Avatar 360 FT-IR). NMR spectra were recorded on a Bruker AV400 spectrometer (400 MHz for ^{1}H-NMR and 100 MHz for ^{13}C-NMR or APT) or a Bruker AV300 spectrometer (300 MHz for ^{1}H-NMR and 75 MHz for ^{13}C-NMR or APT) in the deuterated solvents stated (ESM). ^{1}H and ^{13}C chemical shifts were referenced to internal solvent resonances and reported relative to TMS. High-resolution electrospray (ESI+) mass spectra were registered on a Bruker Daltonics MICROTOF-Q spectrometer using ultra-diluted solutions of the chemical compounds in methanol.

Sample preparation for aggregation assays (Turbidimetry, DLS and TEM)

Samples were prepared from stock solutions of peptide ($A\beta_{17-40}$) and synthesized compounds. Before use, the $A\beta_{17-40}$ stock solution was filtered for 4 minutes at 4 ºC using Ultrafree®-MC filter devices (PVDF 0.22 μM pore size membrane) at 12000 rcf. Then, 50 μM $A\beta_{17-40}$ was mixed with 100 μM compound in PBS buffer and the pH was adjusted to 7-8. All final solutions (including controls) contained 2.5 % DMSO.

Turbidimetry assay

The samples (500 μL) were incubated at room temperature with gentle shaking, and aggregation kinetics were followed by recording the absorbance at 650 nm, every 30 minutes over 8 h, in a Varian Cary 100 Bio spectrophotometer. Quartz cuvettes (Hellma 119F-QS with 10 mm light path) were used for this purpose.

Dynamic Light Scattering

The samples (100 μL) were incubated at room temperature with gentle shaking. Autocorrelation curves (correlograms) were registered at 25 ºC for 48 hours in a DynaPro NanoStar cuvette-based DLS instrument, using Eppendorf UVette plastic cuvettes. This system uses a GaAs laser operating at a nominal wavelength of 658 nm, and a DLS detector operating at 90 degrees. 20 acquisitions (2 s acquisition time) were averaged for each measurement.

Transmission Electron Microscopy

Samples (100 μL) were incubated at 37 ºC for 24 h without shaking. Then, 20 μL-drops were placed on carbon support film on a copper 400 mesh grid and negatively stained with a 2% uranyl acetate solution for 1 min. Excess stain was removed and samples were washed with deionized Milli-Q water and dried at room temperature. TEM images were collected at 60 kV under a JEOL JEM 1010 transmission electron microscope equipped with a Gatan Bioscan digital camera.

Cytotoxicity assay

HeLa cells (ATCC CRM-CCL-2), cultured in Dulbecco's Modified Eagles Medium (DMEM) supplemented with penicillin-streptomycin (100 U/mL and 100 μg/mL, respectively) and 10% fetal bovine serum (all reagents from PAN-Biotech), were aliquoted in 96-well plates (100 μL per well at 3 x 10^5 cell/mL) and incubated for 24 hours (37 ºC and 5% CO_2) in the absence or presence of compound (at concentrations ranging from 0.5 to 200 μM). All wells contained 1% DMSO. After incubation, cell media was carefully removed and each well was refilled with 50 μL of a XTT/electron-coupling agent 500:1 mixture (Cell Proliferation Kit II, Roche). After 4h of incubation, optical density was measured at 450 nm (reference wavelength: 650 nm) in a Synergy HT spectrophotometer plate reader (100 % viability was considered for controls without compound). Half-maximal cytotoxic concentration (CC_{50}) was calculated for Compound 1B, by fitting the viability at each concentration to a dose-response curve with variable Hill slope (Hill1 implemented in Origin Pro 8 software).

Preparation of fibrils of amyloidogenic peptides for fluorescence microscopy assays

For $A\beta_{1-42}$ fibrils formation, $A\beta_{1-42}$ 50 μM solutions were prepared in PBS buffer from peptide stock solutions, and were incubated at 37 ºC for 24 hours without shaking. The same was done with Ac-amylin 8-37. On the other hand, α-PSM1 and α-PSM4 amyloid fibrils (200 μM in Milli-Q water) were obtained as described [23].

Detection of amyloid fibrils by fluorescence microscopy

50 μM amyloid fibrils (obtained as described above) were mixed with 100 μM compound (from compound stock solution) in PBS buffer. All final samples (including controls) contained 5 % DMSO. Samples (100 μL) were incubated at 37 ºC for 24 h without shaking and then centrifuged at 12000 rcf for 15 min at 20 ºC. Supernatants were removed and pellets resuspended in 10 μL PBS. A 2-μL drop of each resuspended sample was placed on a clear glass microscope slide (25 mm x 75 mm) and covered with a 10 mm diameter coverslip. For observation in the fluorescence microscope, a DAPI filter (excitation: 360/40 nm; emission: 470/40 nm) was used in a Leica DMI 6000B multidimensional microscopy system with a 20x microscope objective, 100% fluorescence intensity manager (FIM) and 100-ms exposure time. For ThT staining, a CFP filter (excitation: 436/20 nm, emission: 480/40 nm) was used instead. For each drop, images in 9 chosen-randomly positions were acquired to determine an average

value of the pixel intensity and the percentage of fluorescently marked area. These parameters were calculated with the Fiji (ImageJ) software applying an Auto-Threshold method (Moments) for 8-bit images.

Biofilm formation, staining and observation by fluorescence microscopy

For biofilm formation, cells (*S. aureus* SH1000 strain) were grown in PNG (3.3 g/L peptone, 2.6 g/L NaCl, 3.3 g/L glucose) or TSBg (0.6 g/L tryptic soy broth, 1.5 g/L glucose) culture media at 37 ºC for 24 hours on glass microscope coverslips placed in polystyrene cell culture plates. After incubation, biofilms were fixed with paraformaldehyde 3% and coverslips were placed over an 80 μL-drop of compound 1D (100 μM in H_2O_{mq}, 1% DMSO) and incubated at room temperature for 24 hours in a humidity chamber. Before observation, biofilms were washed (coverslips were immersed in H_2O_{mq} three consecutive times) to remove the excess of compound 1D. For observation in the fluorescence microscope, a DAPI filter (excitation: 360/40 nm; emission: 470/40 nm) was used in a Leica DM4000 B system with a 100x microscope objective, 100% fluorescence intensity manager (FIM) and 40-ms exposure time.

Absorption and emission spectra of compounds 1A-D

Absorption and emission spectra were measured for compounds 1A, 1B, 1C and 1D (30 μM in PBS buffer with 5% DMSO) using 10 mm light path quartz cuvettes (Hellma 119F-QS). For absorption spectra, absorbance was recorded between 250 and 800 nm in a Varian Cary 100 Bio spectrophotometer. Emission spectra (λ_{ex} = 350 nm) were recorded between 380 and 670 nm at 20 ºC in a Varian Cary Eclipse fluorescence spectrophotometer.

Lifetime and quantum yield measurements

For lifetime measurements, the following samples were prepared from compound and peptide stock solutions: compound 1D (30 μM) in the absence or the presence of $A\beta_{1-42}$ fibrils (15 μM) in PBS buffer (final solutions contained 5% DMSO). After 24 hours of incubation at 37 ºC (for $A\beta_{1-42}$/1D sample), nanosecond lifetimes were recorded with a Datastation HUB-B with a nanoLED controller and software DAS6. The nanoLED employed for lifetime measurements was of 340 nm and the data was collected at 466 nm. The lifetime data were fitted using the Jobin-Yvon software package and the Origin Pro 8 program. Quantum yield of compound 1D (30 μM in PBS 5% DMSO) was measured using the Hamamatsu Absolute PL Quantum Yield Measurement System C11347-11.

Water solubility prediction for compounds 1A-D

LogS values at 25 ºC, log(solubility in mol/L), for compounds 1A, 1B, 1C and 1D (-9.6, -9.8, -9.2 and -9.7, respectively) were predicted using *Solubility Predictor* by ChemAxon.

RESULTS AND DISCUSSION

Design of labeled inhibitors

We have chosen Compound 1 (Chart 1) as the scaffold for the design and synthesis of Aβ fluorescent markers because it is the more water soluble [17] and less cytotoxic of the amyloid aggregation inhibitors previously described [16]. The fluorescent dye pyrene has been selected to label Compound 1 because of its high fluorescence quantum yield. 1-pyrenemethylamine has been used as reactant in the coupling reaction because it allows a fine control of its chemical reactivity. While the residues of $A\beta_{1-40}$ that interact with Compound 1 have been determined [17], the atoms of Compound 1 that are engaged in the interaction are not known. Therefore, we have synthesized 4 derivatives of Compound 1 (Compounds 1A, 1B, 1C and 1D) having the fluorescent dye located in different positions or joined with linkers of different length (Chart 1) hoping to retain the amyloid binding properties in at least some of them. As shown in Fig. S2 in the ESM, compounds 1A, 1B, 1C and 1D display large Stokes shifts ($\Delta\lambda >$ 100 nm), their absorption and emission spectra having maxima at approximately 355 nm and 470 nm, in PBS buffer.

Synthesis of fluorescent derivatives of compound 1

Schemes 1 and 2 show the synthetic routes to fluorescent derivatives of Compound 1, adapted from different methods found in the literature [24–27]. For synthesis of compounds 1A and 1B (Scheme 1), the initial step was the nucleophilic attack of 2-aminotiophene derivative 2 to the cyclic anhydrides 3 and 4, respectively, to obtain compounds 5 and 6, which were subsequently transformed into dicarboxylic acids 7 and 8 by alkaline hydrolysis. Higher yields were obtained for this saponification when it was conducted at 36 ºC than when using reflux. The latter conditions led to the formation of byproducts, probably as a result of amide saponification. The cyclization reaction with acetic anhydride that leads to the key lactone intermediates 9 and 10 was performed at room temperature. When it was carried out using reflux conditions, as described in the literature [24], unwanted byproducts 9S and 10S (shown in Fig. S1 in the ESM) were formed. Crude products 9 and 10 were used in the next step without purification. Compounds 1A and 1B were obtained with moderate yields using DCC and HOBT as coupling reagents for the amide bond formation.

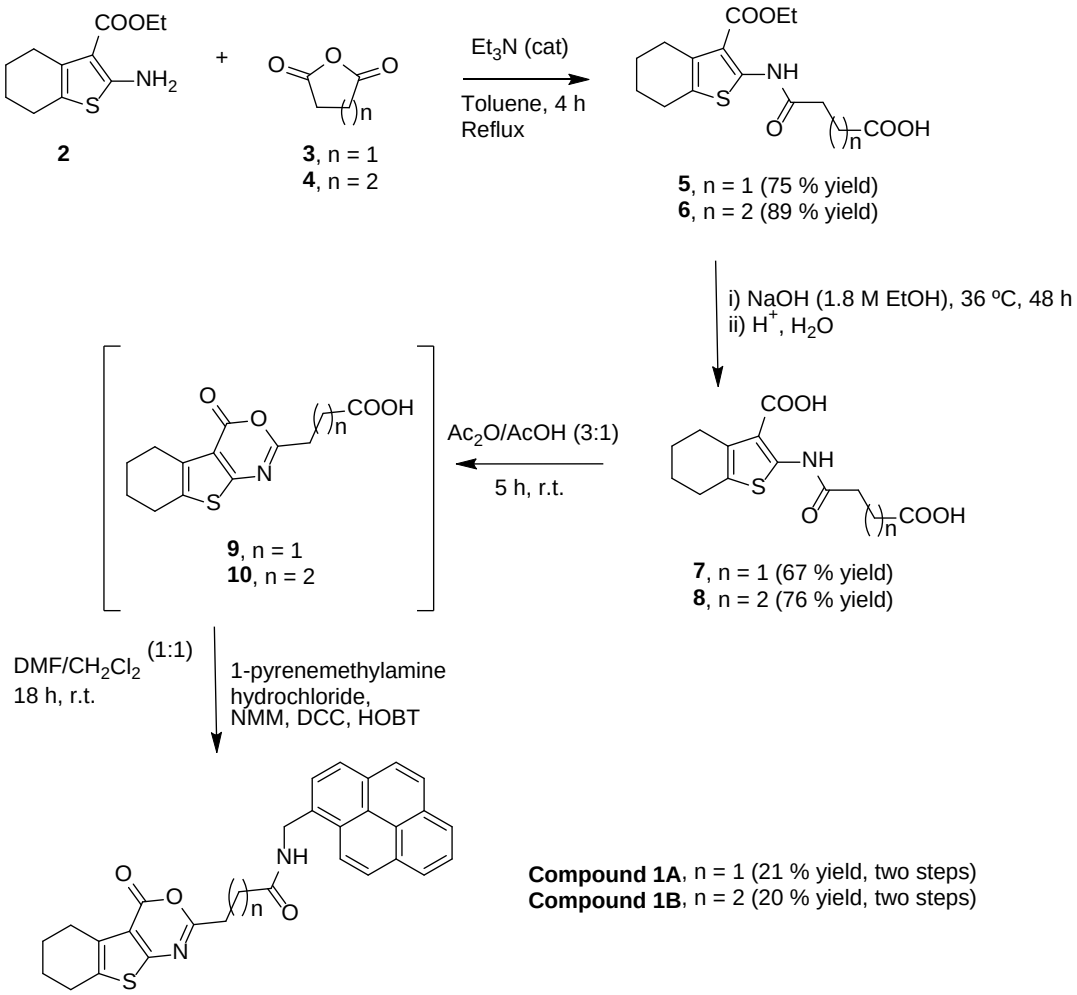

Scheme 1. Synthesis of compounds 1A and 1B

Compounds 1C and 1D were prepared as shown in Scheme 2. Synthesis of starting compound 12 was done with 76 % overall yield following methods found in the literature [28, 29]. 2-aminothiophenes 13 and 14 were obtained by Gewald reaction [30] between cyclohexanones 11 and 12, respectively, ethyl cyanoacetate and powdered sulfur. By saponification of 13 and 14, only one ethyl carboxylate was hydrolyzed for all tested conditions leading to compounds 15 and 16. After the acetylation step, the pyrene fluorescent dye was attached to 17 and 18 using HOBT and EDC as coupling agents. Compounds 19 and 20 were hydrolyzed with the less nucleophilic base lithium hydroxide to minimize by-product formation due to amide saponification. Finally, cyclization of 21 and 22 with acetic anhydride led to compounds 1C and 1D with good yields. In these cyclization conditions, the more accessible amide nitrogen of 22 was acetylated as it is observed in compound 1D.

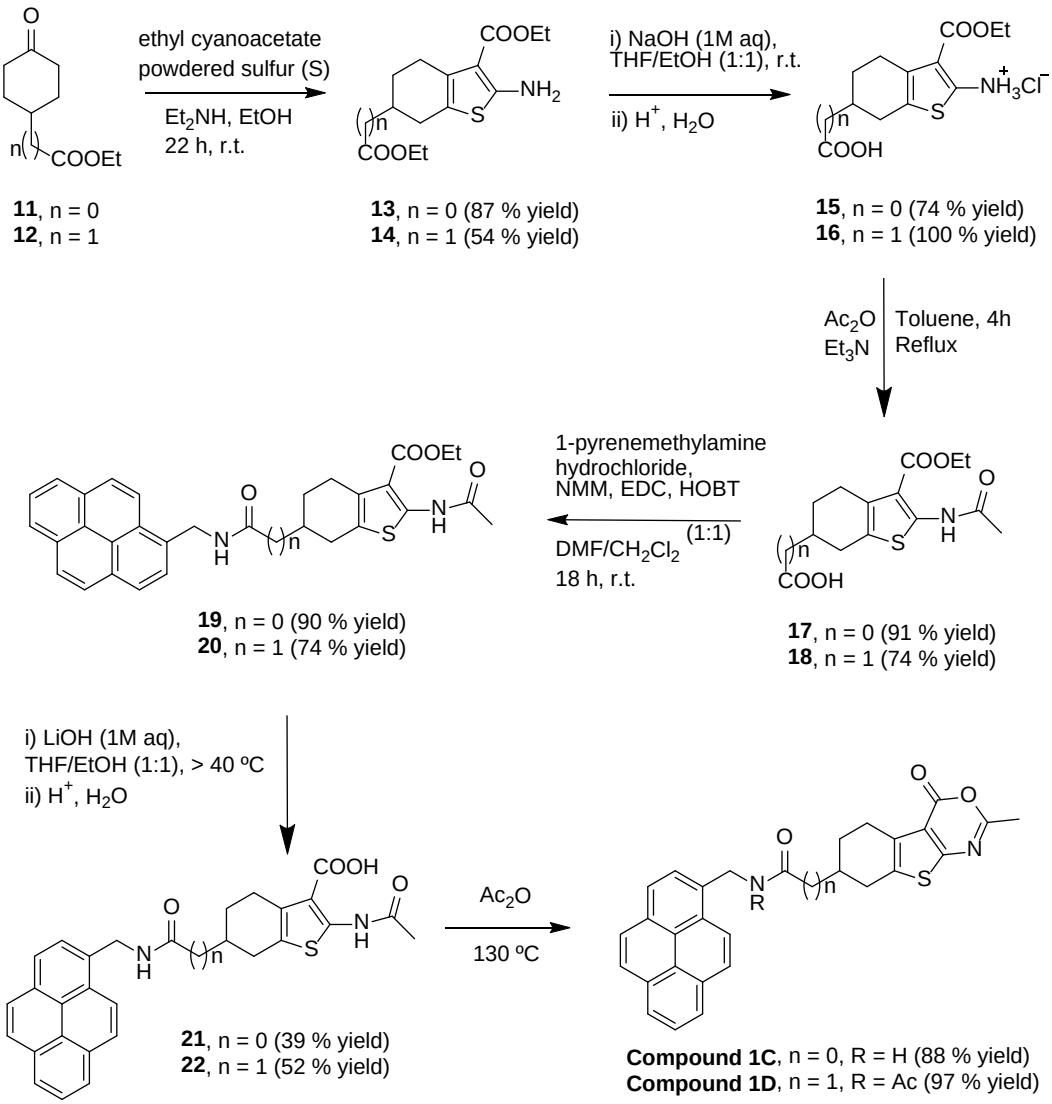

Scheme 2. Synthesis of compounds 1C and 1D

Anti-aggregational activity of fluorescent derivatives of Compound 1

In a previous study [16] we tested 11250 compounds from two large commercial libraries as inhibitors of the aggregation of $A\beta_{17-40}$ using a ThT fluorescence-based high throughput screening assay, which allowed to identify 35 tentative inhibitors. In order to discard false positives arising from fluorescence quenching, a turbidimetry assay was subsequently done, and 4 inhibitors were finally selected that were confirmed using transmission electron microscopy images. On the other hand, to evaluate initially whether the synthesized derivatives of Compound 1 could be used as fluorescent markers of Aβ fibrils we have first tested them as aggregation inhibitors. Because the emission maximum of the four synthesized compounds in aqueous PBS buffer occurs at practically the same wavelength as that of Aβ-bound ThT (see Fig. S2 in the ESM and reference 18), the classical ThT aggregation assay couldn´t be used. Instead,

turbidimetry, dynamic light scattering and transmission electron microscopy assays have been conducted.

The turbidity assay is easy to perform and offers an initial indication of the inhibitory capacity of the compounds, which has to be confirmed afterwards by additional tests. The assay is based on the apparent enhancement of absorbance that takes place when aggregates or other insoluble particles are formed in a solution. To follow aggregation kinetics, the absorbance at 650 nm of $A\beta_{17-40}$ aqueous samples in presence or absence of synthesized compounds 1A, 1B, 1C and 1D was monitored every 30 minutes. As the assay is noisy and the level of aggregation attained for the control kinetics run without compounds shows large variation (see Fig. 1 below; also Fig. 2 in reference [16]) individual experiments should not be averaged. Instead, their statistical significance is best assessed by Paired t-tests. The kinetics of turbidity enhancement displayed in Fig. 1 indicate that the four synthesized fluorescent compounds and parent Compound 1 significantly slow down the aggregation of the amyloid peptide ($p < 0.002$ in all cases). Therefore, compounds 1A, 1B, 1C and 1D are likely to interact with amyloid fibrils, as we expected, for at least some of them, from their design.

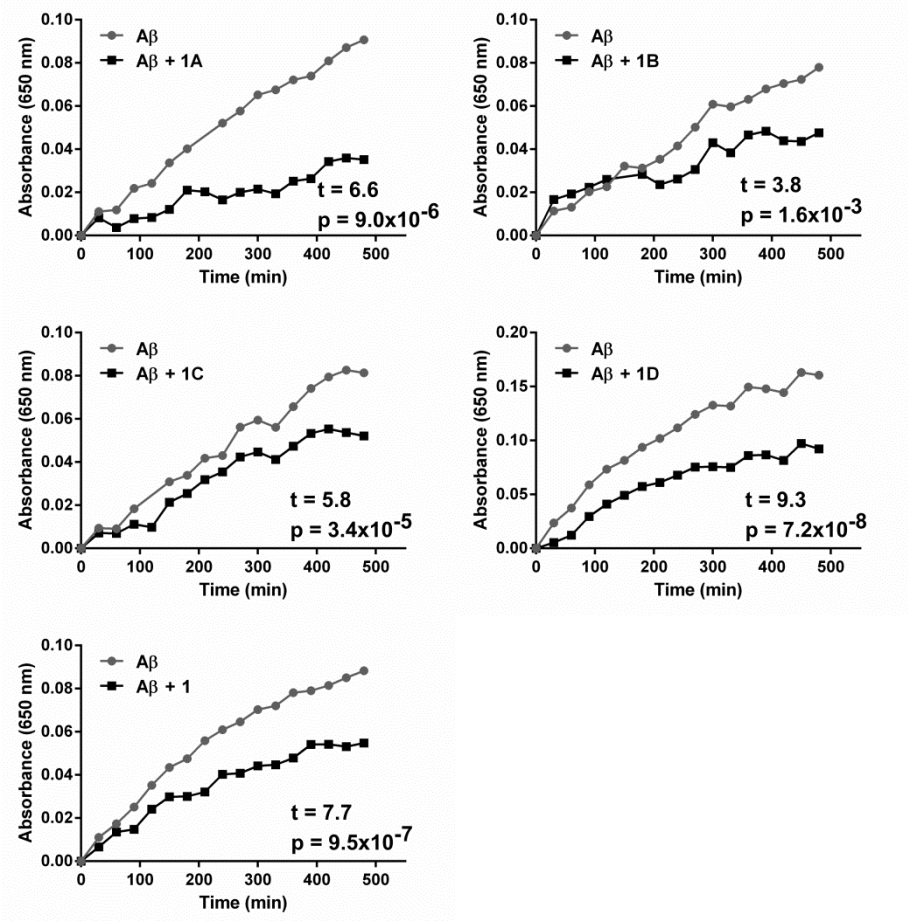

Fig. 1 Turbidimetric monitorization of $A\beta_{17-40}$ (50 μM) aggregation kinetics in the absence (gray circles) and the presence (black squares) of compounds 1, 1A, 1B, 1C and 1D (100 μM). Statistic results (t-statistic and p-value) of Paired t-tests are shown for individual representative experiments.

Dynamic light scattering (DLS) [31] has been used to provide additional evidence of the inhibitory effect of the fluorescence derivatives on Aβ aggregation. In DLS experiments, Brownian motion of particles suspended in a liquid is measured in terms of the translational diffusion coefficient, which is inversely related with their size. Correlograms (correlation curves) provide qualitative information about the mean size of the particles in suspension: the slower the decay, the larger the particle. Thus, larger Aβ insoluble aggregates must delay more the decay of the correlation curves. Correlograms of aqueous samples of $A\beta_{17-40}$ in the presence and absence of Compound 1 measured at different times of incubation (Fig. 2a) reveal that aggregates size increases with incubation time and that, for every incubation time, aggregates size was smaller in presence of Compound 1, confirming that Compound 1 reduces amyloid beta aggregation. DLS experiments with synthesized compounds 1A, 1B, 1C and 1D couldn't be analyzed in the same way because of their low solubility in water due to the pyrene moiety (computationally predicted logS values are around -9.6, see Materials and Methods,). In fact, Fig. 2b shows that, at zero incubation time, the particles in suspension resulting from precipitation of the synthesized fluorescent compounds in PBS buffer (colored curves) were larger than the initial amyloid aggregates (black curve). However, as the aggregation of Aβ progressed, the particle size of all samples increased in such a way that, at 48 hours of incubation, aggregates of $A\beta_{17-40}$ samples in the presence of compounds 1A, 1B, 1C and 1D were smaller than those of $A\beta_{17-40}$ samples without compound (Figure 2c). Therefore DLS analysis also indicates that compounds 1A, 1B, 1C and 1D inhibit the aggregation of $A\beta_{17-40}$.

Finally, transmission electron microscopy (TEM) images of $A\beta_{17-40}$ fibrils were acquired to compare the morphology of the amyloid aggregates formed in the presence or absence of fluorescent compounds 1A, 1B, 1C and 1D or parent Compound 1 (Fig. 3). When $A\beta_{17-40}$ was incubated alone, TEM images taken after 24 hours of incubation at 37 ºC showed a meshwork of aggregates so dense that isolated fibrils could not be observed. In contrast, in amyloid peptide samples incubated in the presence of these compounds, the fibrillary net was more clear and isolated fibrils could be detected that were similar to those formed in presence of the inhibitory parent Compound 1. Thus, turbidimetry, DLS and TEM assays indicate that the four fluorescent derivatives of Compound 1 interact with Aβ aggregates and give grounds to the possibility of using 1A, 1B, 1C and 1D as Aβ fibrils fluorescent stains.

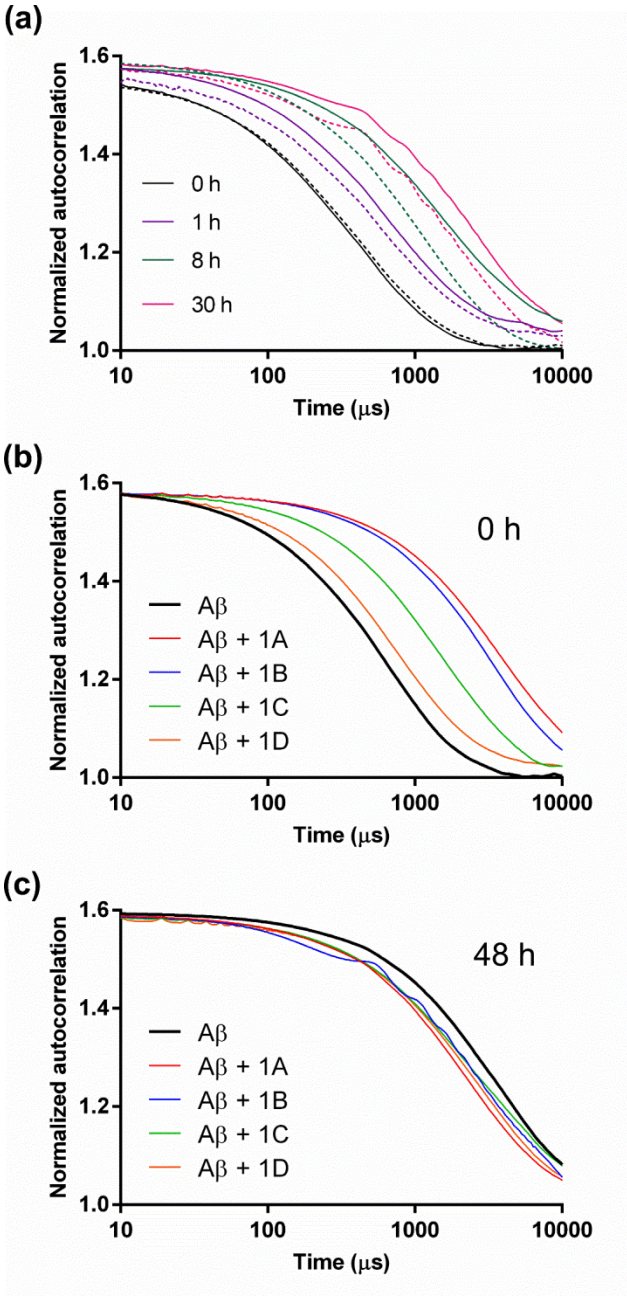

Fig. 2 Dynamic light scattering monitorization of the aggregation kinetics of $A\beta_{17-40}$ (50 μM) in the presence and absence of the studied compounds (100 μM). a) Truncated correlograms measured at different incubation times (see the legend) of $A\beta_{17-40}$ samples in the absence (solid line) and the presence (dashed line) of Compound 1. b) Truncated correlograms measured at zero incubation time of $A\beta_{17-40}$ samples in the absence and the presence of compounds 1A, 1B, 1C and 1D (see the legend) revealing the presence of compound aggregates due to poor solubility. c) Truncated correlograms measured at 48 h incubation time of $A\beta_{17-40}$ samples in the absence and the presence of compounds 1A, 1B, 1C and 1D (see the legend).

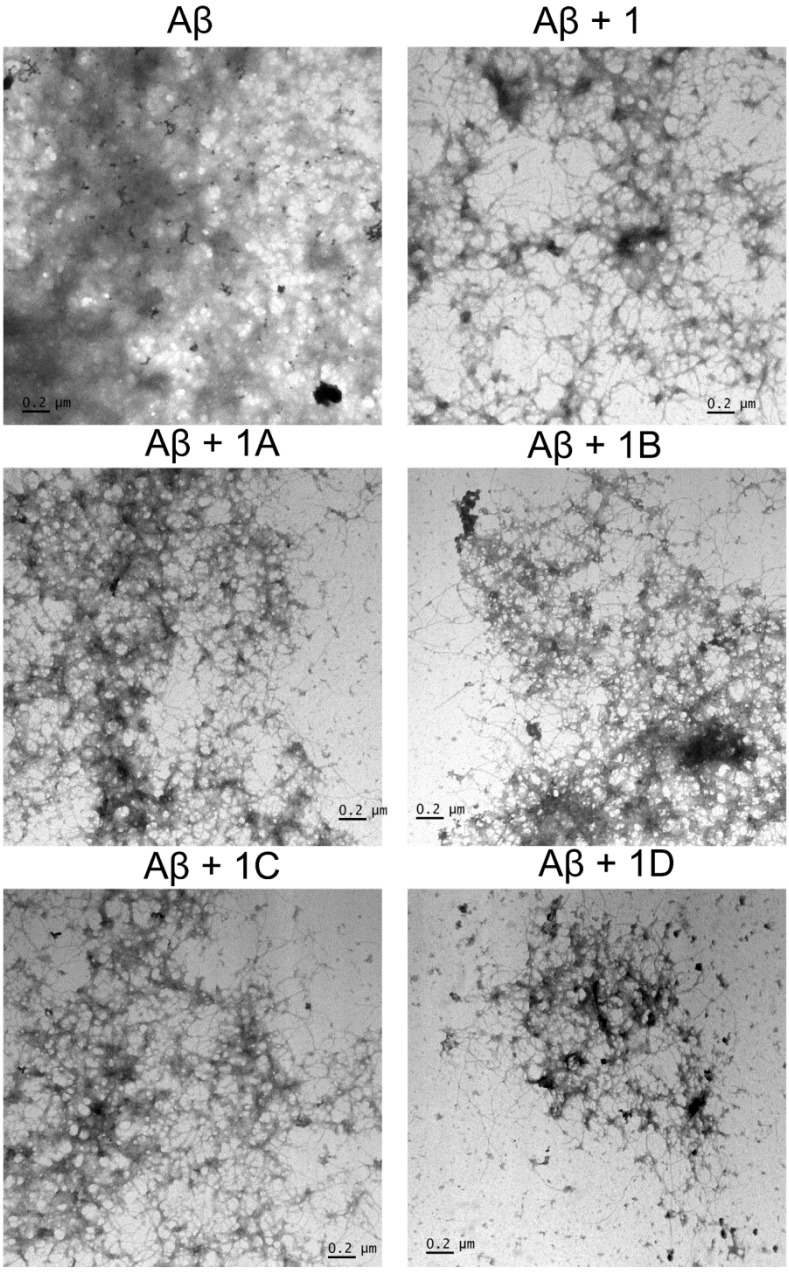

Fig. 3 Morphology of $A\beta_{17-40}$ insoluble aggregates. Transmission electron microscopy images (negative stain) of $A\beta_{17-40}$ (50 μM) samples, with or without aggregation inhibitors (100 μM), acquired after incubation at 37 ºC for 24 h. Scale bar = 0.2 μm.

Cytotoxicity of the compounds

Because compounds 1A, 1B, 1C and 1D reduced $A\beta_{17-40}$ fibrillar growth, we have evaluated their cytotoxicity to obtain a preliminary indication of their potential as labeling agents in living tissues. For that purpose, a cytotoxicity assay of the four synthesized compounds was performed by measuring HeLa cells viability after 24 hours incubation in presence of 1A, 1B, 1C or 1D. The toxicity curves used to calculate half-maximal cytotoxic concentrations (CC_{50}) of the synthesized fluorescent compounds are represented in Fig. 4. Due to the low solubility of the tested compounds, 200 μM was

the highest concentration evaluated. The most toxic compound was 1B (CC_{50} = 112 μM). The three other compounds, 1A, 1C and 1D, with CC_{50}> 200 μM, are less toxic for HeLa cells than the unlabeled, parent Compound 1 (CC_{50} = 184 μM) [16].

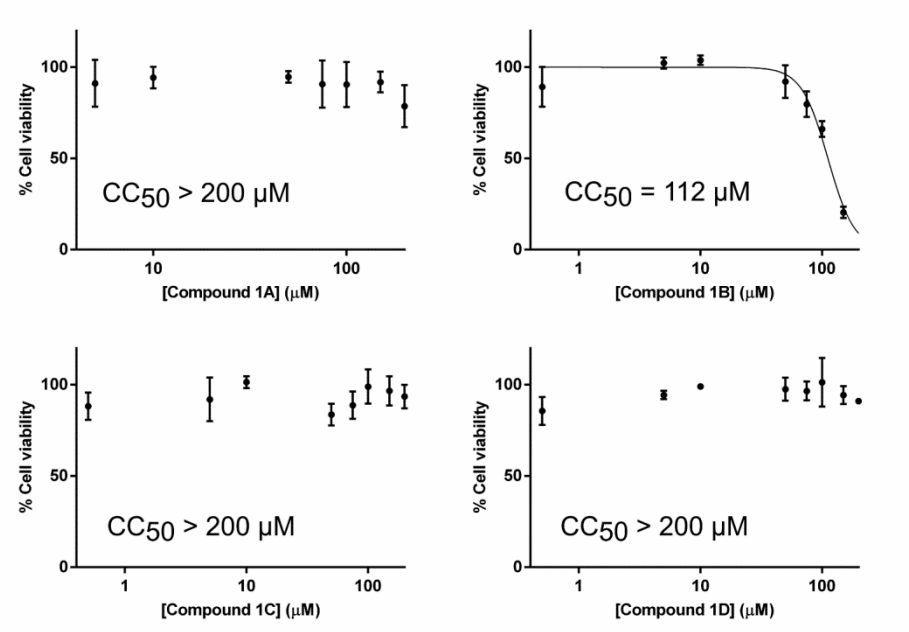

Fig. 4 Cell viability of HeLa cells (3 x 10^5 cell/mL) treated with different concentrations of compounds 1A, 1B, 1C and 1D. Mean ± SD (n = 3) is shown for every compound concentration. CC_{50} indicates the compound concentration that cause death to 50 % of cells (50 % viability) according to the fit of the experimental data.

Use of compound 1D for the detection of $A\beta_{1-42}$ fibrils by fluorescence microscopy

Since compounds 1A, 1B, 1C and 1D have appropriate fluorescent properties with high Stokes shifts and they seem to interact with Aβ aggregates, fluorescence microscopy can be used to detect amyloid fibrils resulting from Aβ aggregation. For that purpose, aqueous samples of compound (100 μM) and $A\beta_{1-42}$ fibrils (50 μM) were incubated for 24 h at 37 ºC, and insoluble fluorescently labeled amyloid aggregates were analyzed by fluorescence microscopy. In view of the spectroscopic properties of the compounds, a DAPI filter (ex: 360/40 nm, em: 470/40 nm) was used. Due to the poor solubility of the synthesized fluorescent probes, a background fluorescent signal was observed when they were incubated without peptide. Compound 1D gave the lowest background signal, which agrees with its greater solubility as detected in DLS experiments (Fig. 2b) and with other visual observations (not shown), so it was selected for this study. To evaluate the ability of compound 1D as fluorescent marker of $A\beta_{1-42}$ fibrils, we first verified that $A\beta_{1-42}$/1D samples generated a higher fluorescent signal than the background observed for compound samples without peptide. A quantitative comparison was made by calculating the average percentage of fluorescently labeled area in microscope images

of $A\beta_{1-42}$/1D and compound 1D alone samples (see representative images in Figs. 5a and 5b). The percentages of fluorescently marked area (means of three duplicated experiments ±SD) were 6.55 ±1.13 and 0.96 ±0.26, for $A\beta_{1-42}$/1D samples and compound 1D alone, respectively. Those percentages are statistically different with a confidence level of $p < 0.001$. That the fluorescence signal observed in the $A\beta_{1-42}$/1D samples was due to the interaction between peptide and probe was indicated by the signal concentration dependence: fluorescence values decrease both with decreasing concentrations of 1D at constant $A\beta_{1-42}$ concentration (Fig. 6a) and with decreasing peptide concentration at constant concentration of 1D (Fig. 6b). On the other hand, to demonstrate that the molecular fragment of 1D responsible for the interaction with $A\beta_{1-42}$ (and for the resulting fluorescent identification) is the one derived from parent compound 1 and not the pyrene fluorescent label, the fluorescence intensity of $A\beta_{1-42}$ fibrils incubated in presence of 1D or pyrene was compared. To do that, the average pixel intensity of the microscope images, related with the sensitivity in Aβ staining of the two different compounds, was determined. As expected from the high hydrophobicity of the pyrene moiety, Aβ fibrils were fluorescently marked but the obtained intensity observed in presence of 1D was 3.2 times higher (Fig. 7). That Compound 1D interacts with $A\beta_{1-42}$ fibrils through its inhibitor moiety, as per design, is also indicated by the fact that its fluorescence lifetime hardly changes upon binding: 41 ns in PBS 5% DMSO versus 39 ns when bound to the fibrils. It is also suggested by the fact that the emission maximum does not change either (not shown).

Selectivity and sensitivity of compound 1D for the detection of amyloid fibrils

To evaluate the selectivity of compound 1D as Aβ fibrils fluorescent stain, α-synuclein and amylin amyloid fibrils, as well as bovine serum albumin (BSA), were incubated with compound 1D. BSA was chosen as an example of soluble, non amyloidogenic protein because it contains hydrophobic pockets that could interact with compound 1D. The signal value (percentage of fluorescently marked area) of BSA/1D sample before 24 hours of incubation was not significantly different from background signal of 1D sample (Fig. 8a). However, microscope images of 1D and of BSA/1D samples were qualitatively different suggesting that soluble BSA interacts with compound 1D in some way and makes it precipitate as smaller and more homogeneous particles (see representative images in Fig. 5b and 5e). Something similar occurred with α-syn/1D 24 h-incubated sample. Although no amyloidogenic fibrils of this protein are formed in 24 h, compound 1D appears to interact with soluble α-syn as with BSA, giving rise to a more homogeneous background (not shown). Importantly, the low reproducibility in α-syn aggregation results in a low reproducibility in the staining of preformed α-syn fibrils, which, when a good aggregation is achieved, are stained by 1D similarly to Aβ. On the other hand, amylin fibrils were also marked with compound 1D in the same manner as Aβ (Fig. 8b). Therefore, compound 1D is not specific of Aβ aggregates but can label a variety of amyloid fibrils. The intensity of $A\beta_{1-42}$ and amylin fibrils stained with 1D has been compared to that of fibrils stained with ThT. To record the emission

fluorescence of ThT samples a CFP filter (ex: 436/20 nm, em: 480/40 nm) was used, whose excitation and emission wavelengths fit with ThT spectroscopic properties. Results presented in Fig. 7 show that compound 1D stained $A\beta_{1-42}$ and amylin insoluble fibrils almost as efficiently as ThT, generating, in our staining conditions, fluorescent signals 0.6 and 0.7 times those of ThT, respectively. To sum up, compound 1D, a pyrene labeled inhibitor of $A\beta_{1-42}$ aggregation, can be used to monitor by fluorescence microscopy the presence of $A\beta_{1-42}$ fibrils as well as those of α-synuclein and amylin. On the other hand, compound 1D can be efficiently excited in the UV region and displays a large Stokes shift: $\Delta\lambda$ = 116 nm in our microscope filter conditions, and $\Delta\lambda$ = 186 nm if excitation is conducted at 280 nm (Fig. 9). It thus provides an alternative spectroscopic window for the detection of amyloid fibrils and facilitates minimizing crosstalk between the excitation source and the fluorescent emission [32]. In addition, compound 1D is photostable, its fluorescence is insensitive to changes in pH (see Fig. S3 in the ESM) showing a quantum yield of 0.23 in PBS 5% DMSO, and its low cytotoxicity allows its use for *in vivo* staining. Table 1 compares properties of compound 1D with those of commonly employed amyloid stains Thioflavin T and Congo Red.

Table 1. Comparison of compound 1D, Thioflavin T and Congo Red amyloid stain properties.

	Compound 1D	**Thioflavin T**	**Congo Red**
Amyloid detection method	Fluorescence	Fluorescence	Absorption/Dichroism
Absorption maximum	350 nm	445 nm[a]	490 nm[b]
Emission maximum	466 nm	485 nm[a]	N/A
Stokes shift	116 nm	40 nm	N/A
Aβ selectivity[c]	No	No	No
Fluorescence intensity (relative to Aβ/1D interaction)	1.0	1.7	N/A
Useful pH range	2.0 – 10.0[d]	3.0 – 8.5[e]	> 5.0[b]
Water solubility (logS)	-9.7[f]	-1.8[g]	-1.4[h]

N/A value not available (not related with the detection method).
[a]Reference [33].
[b]Reference [34].
[c]Specificity for Aβ staining in relation to other amyloid fibrils.
[d]Assayed range (Fig. S3).
[e]Reference [35].
[f]Computationally predicted by ChemAxon's Solubility Predictor.
[g]Obtained from Merck Millipore product information.
[h]Reference [36].

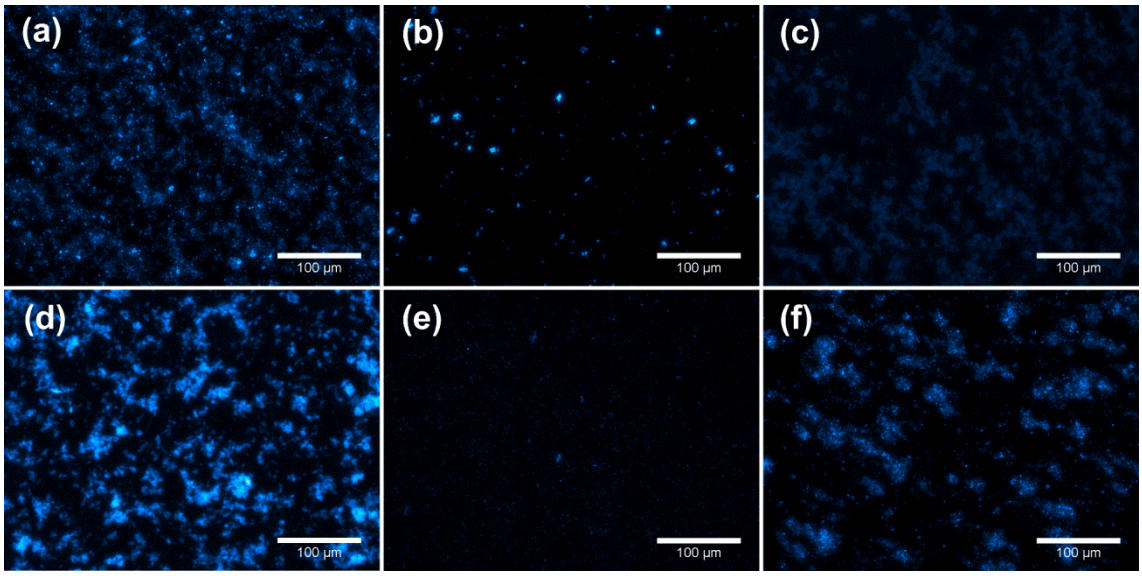

Fig. 5 Fluorescence microscope images of pellets obtained after 24 h of incubation at 37 ºC for the following aqueous (PBS) samples. a) $A\beta_{1-42}$ fibrils (50 µM) and compound 1D (100 µM). b) Compound 1D (100 µM) alone. c) $A\beta_{1-42}$ fibrils (50 µM) and fluorescent dye (1-Pyrenemethylamine hydrochloride, 100 µM). d) $A\beta_{1-42}$ fibrils (50 µM) and ThT (100µM). e) BSA (50 µM) and compound 1D (100 µM). f) α-syn fibrils (50 µM) and compound 1D (100 µM). Scale bar = 100 µm.

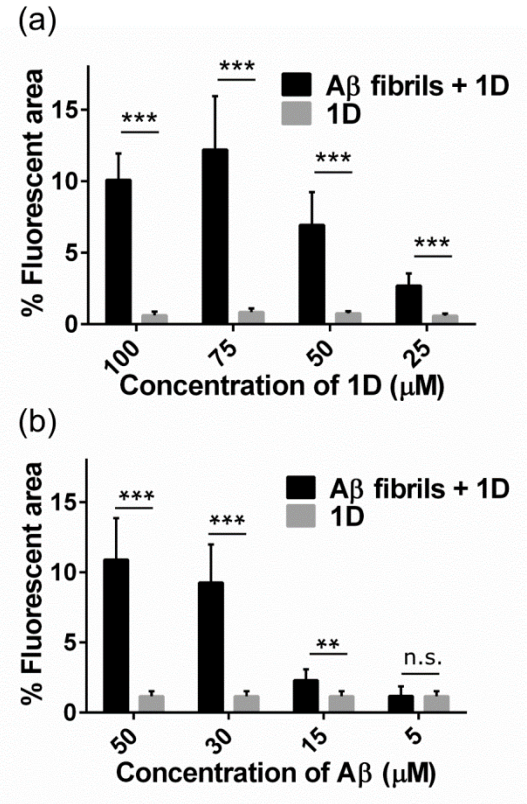

Fig. 6 Quantitative analysis and statistical comparison of the percentage of fluorescent area in the microscope images acquired for the indicated samples (for their pellets) after incubation at 37 ºC for 24 h. a) Compound 1D (different concentrations) in the presence (black column) and absence (gray column) of $A\beta_{1-42}$ fibrils (50 μM). b) Compound 1D (100 μM) in the presence (black column) and absence (gray column) of $A\beta_{1-42}$ fibrils (different concentrations). Statistical differences were evaluated by Student's t-test (*** means $p < 0.001$, ** means $p < 0.01$ and n.s. means non-significant differences). Error bars represent SD of the measurement.

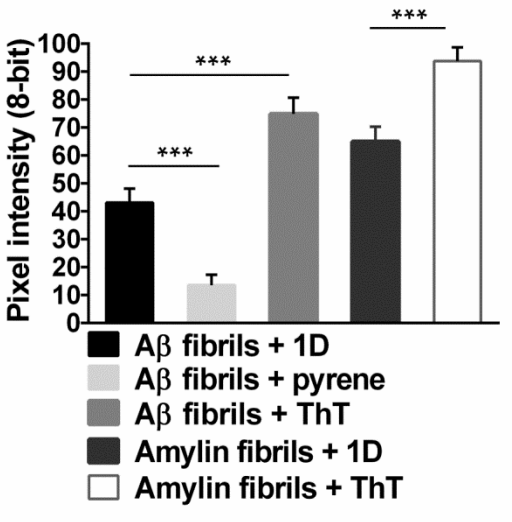

Fig. 7 Quantitative analysis and statistical comparison of the pixel intensity in the microscope images acquired for the indicated samples (for their pellets) after incubation at 37 ºC for 24 h: $A\beta_{1-42}$ fibrils (50 μM) in the presence of 100 μM 1D (black column), 100 μM pyrene fluorescent dye (light gray column) or 100 μM ThT (gray column). Amylin fibrils (50 μM) in the presence of 100 μM 1D (dark gray column) or 100 μM ThT (white column). Statistical differences were evaluated by Student's t-test (*** means $p < 0.001$). Error bars represent SD of the measurement.

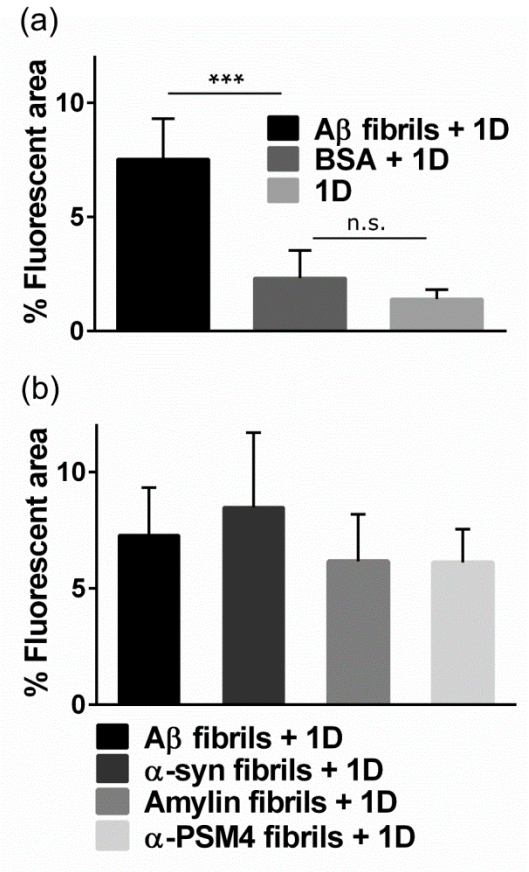

Fig. 8 Quantitative analysis and statistical comparison of the percentage of fluorescent area in the microscope images acquired for the indicated samples (for their pellets) after incubation at 37 ºC for 24 h. a) Compound 1D (100 μM) in the absence (light gray column) and presence of 50 μM $A\beta_{1-42}$ fibrils (black column) or 50 μM soluble BSA (dark gray column). b) Compound 1D (100 μM) in the presence of fibrils (50 μM) of $A\beta_{1-42}$ (black column), α-syn (dark gray column), amylin (light gray column) and α-PSM4 (pale gray column). Statistical differences were evaluated by Student's t-test (*** means $p < 0.001$ and n.s. means non-significant differences). Error bars represent SD of the measurement.

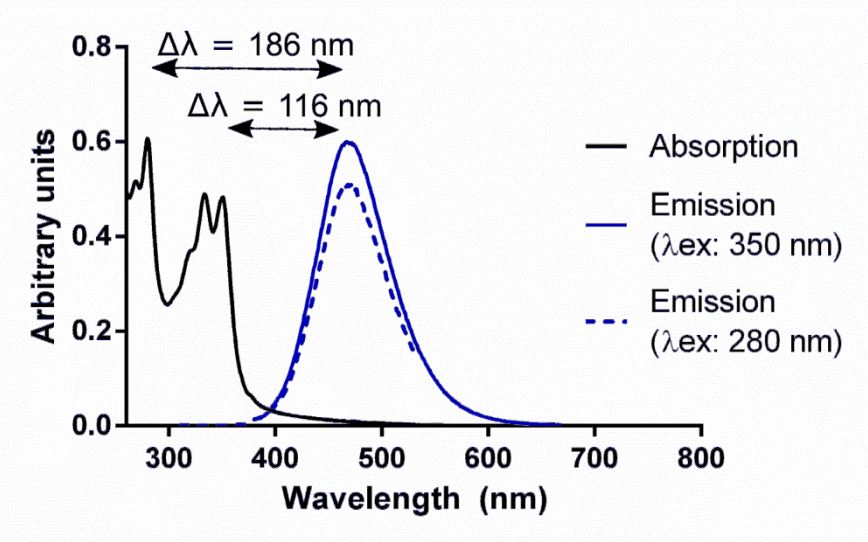

Fig. 9 Stokes shifts of compound 1D. Absorption and emission (excitation wavelength: 350 nm, blue solid line, and 280 nm, blue dashed line) spectra obtained in PBS buffer (30 μM, 5% DMSO)

Use of compound 1D to detect amyloid fibrils of α-PSM4 by fluorescence microscopy

In *Staphylococcus aureus*, phenol soluble modulins (PSMs) peptides are known to be important constituents of the extracellular biofilm matrix that provide the bacteria with resistance to chemicals and host immune response. From all PSMs studied (α-PSM1-4), only α-PSM1 and α-PSM4 showed amyloidogenic properties, with α-PSM4 having the greater ability to form ordered amyloid fibrils [23].

We have evaluated the ability of fluorescent compound 1D to stain α-PSM1 and α-PSM4 fibrils by fluorescence microscopy in the same manner as for the other studied peptides. α-PSM4 fibrils were stained by 1D similarly to Aβ and the other amyloidogenic fibrils (Fig. 8b). However, compound 1D showed a lower sensitivity for α-PSM1 fibrillar solution, generating a signal 2.9 times less intense than for α-PSM4 fluorescently stained fibrils (Fig. 10), which correlates well with the much weaker amyloidogenic properties of α-PSM1 peptide, as previously described [23].

Therefore, compound 1D could be a useful tool to analyze the amyloid nature of PSMs fibrils.

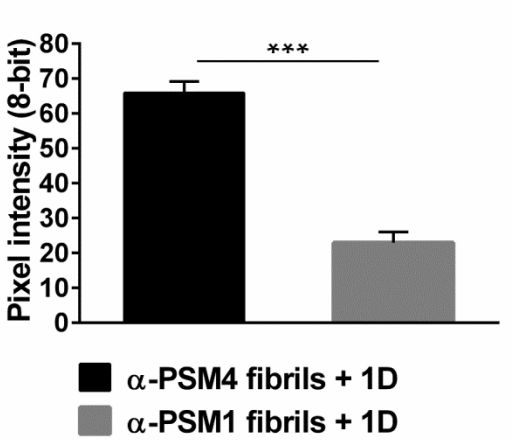

Fig. 10 Quantitative analysis and statistical comparison of the pixel intensity in the microscope images acquired for the following samples (for their pellets) after incubation at 37 ºC for 24 h: α-PSM4 fibrils (50 μM) in the presence of 100 μM 1D (black column) and α-PSM1 fibrils (50 μM) in the presence of 100 μM 1D (gray column). Statistical differences were evaluated by Student's t-test (*** means $p < 0.001$). Error bars represent SD of the measurement.

Use of compound 1D to analyze the amyloid nature of *Staphylococcus aureus* extracellular biofilm matrix

Biofilm formation is universal for all bacteria but the nature of the biofilm matrix composition varies by strain, physiological state and nutrient availability. *S. aureus* SH1000 biofilms grown in peptone-NaCl-glucose (PNG) media develop an extracellular matrix composed of amyloid fibrils of phenol soluble modulins [22]. However, when grown in tryptic soy broth supplemented with glucose (TSBg), the biofilm matrix lacks amyloid and becomes less stable.

We have tested compound 1D as fluorescent stain for amyloid-like extracellular matrix using *S. aureus* SH1000 biofilms grown in PNG media and subsequently exposed to an aqueous solution of the studied compound. Fluorescence microscopy images showed a clear interaction between compound 1D and the amyloid extracellular components (PSMs fibrils) of the biofilm matrix (Fig. 11a). Interestingly, this interaction was not observed for *S. aureus* SH1000 biofilms grown in TSBg media (Fig. 11b), indicating that compound 1D is useful to stain PSM-derived biofilm matrix and therefore to distinguish between *S. aureus* biofilms that contain or lack amyloid fibrils.

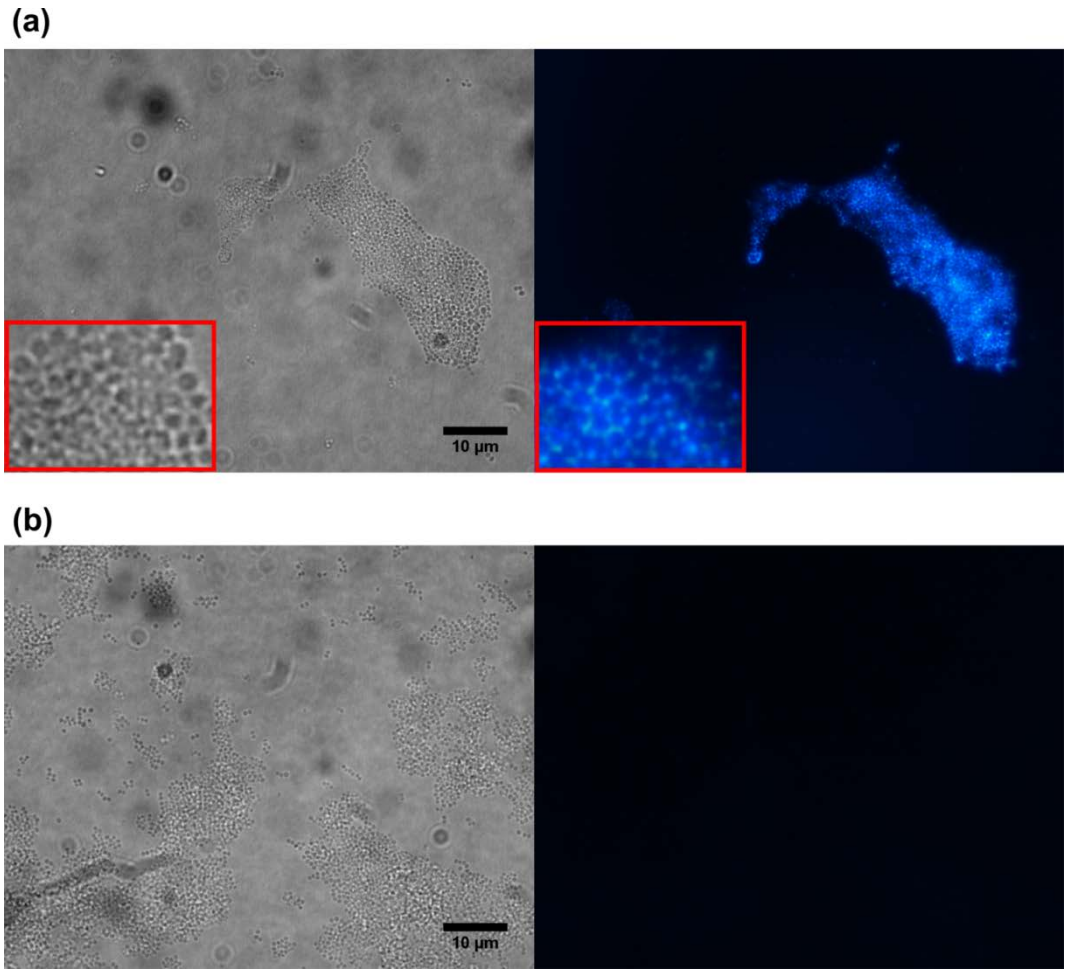

Fig. 11 Microscope images (left: bright field, right: DAPI fluorescent filter) of *S. aureus* SH1000 biofilms grown in a) PNG culture media (zoomed inset) or b) TSBg culture media and incubated with 100 µM 1D. Scale bar = 10 µm.

CONCLUSIONS

Synthetic procedures have been developed to attach pyrene, a high quantum yield fluorescent dye, to different positions of Compound 1, a previously reported inhibitor of Aβ peptide aggregation. The resulting fluorescent compounds 1A, 1B, 1C and 1D have been tested in terms of sensitivity and selectivity for the fluorescent staining of insoluble amyloid fibrils. Turbidimetry, DLS and TEM assays indicate that the four synthesized compounds interact with $A\beta_{17-40}$ aggregates in a similar way as the parent Compound 1. The more water soluble compound 1D was selected to evaluate its ability as $A\beta_{1-42}$-fibrils fluorescent marker. Fluorescence microscopy monitoring reveals that compound 1D can be used to stain $A\beta_{1-42}$ fibrils as well as those formed by other amyloidogenic peptides such as amylin or α-synuclein, offering a sensitivity close to that of ThT staining. Compound 1D displays a conveniently large Stokes shift, it is photostable, shows a pH-independent fluorescence quantum yield and it is not cytotoxic. Furthermore, compound 1D can stain the amyloidogenic components (PSMs) of the *Staphylococcus aureus* biofilm matrix and allows distinguishing by direct staining biofilms that contain amyloid fibrils from those lacking them. Because chronic biofilm-associated infections caused by *Staphylococcus aureus* often lead to significant increases in morbidity and mortality, a better understanding of the composition of staphylococcal biofilm matrix, for which compound 1D constitutes a novel tool, is imperative to generate more accurate treatment strategies.

ASSOCIATED CONTENT

Electronic Supplementary Material (ESM): Synthetic procedures, characterization, ^{1}H-NMR spectra and ^{13}C-NMR spectra of all synthesized compounds. Additional figures cited in the text (Figures S1 to S3).

ABBREVIATIONS

AD, Alzheimer's disease; Aβ, amyloid beta; APP, β-amyloid precursor protein; ThT, Thioflavin T; PSMs, phenol soluble modulins; DLS, dynamic light scattering; TEM, transmission electron microscopy; CC_{50}, half-maximal cytotoxic concentration; BSA, bovine serum albumin; α-syn, α-synuclein; DMEM, Dulbecco's Modified Eagles Medium; DAPI, 4',6-Diamidine-2'-phenylindole; GFP, green fluorescent protein; PNG, peptone-NaCl-glucose media; TSBg, tryptic soy broth supplemented with glucose; PBS, phosphate-buffered saline; DMSO, dimethyl sulfoxide; DCC, N,N'-Dicyclohexylcarbodiimide; EDC, 1-Ethyl-3-(3-dimethylaminopropyl)carbodiimide, HOBT, 1-Hydroxybenzotriazole.

COMPLIANCE WITH ETHICAL STANDARDS

The authors declare that they have no conflict of interest.

REFERENCES

1. Selkoe DJ. Alzheimer's Disease. Cold Spring Harb Perspect Biol. 2011;3:a004457
2. Holtzman DM, Morris JC, Goate AM. Alzheimer's disease: the challenge of the second century. Sci Transl Med. 2011;3:77sr1
3. Selkoe DJ, Morris JC, Petersen RC, Lewis J, Davies P, Maloney AJ, Whitehouse PJ, Small DH, Mok SS, Bornstein JC, Davies CA, Mann DM, Sumpter PQ, Yates PO, Terry RD, Dickson DW, Sze CI, Masliah E, Hsia AY, Mucke L, Naslund J, Kuo Y-M, McLean CA, Lue LF, Bookheimer SY, Reiman EM, Polvikoski T, Selkoe DJ, Chen G, Larson J, Lynch G, Games D, Seubert P, Moechars D, Chapman PF, Fitzjohn SM, Johnson-Wood K, Gravina SA, Walsh D, Lambert MP, Hartley D, Stephan A, Laroche S, Davis S, Dewachter I, Dodart JC. Alzheimer's disease is a synaptic failure. Science. 2002;298:789–791
4. Alzheimer A. Uber eine eigenartige Erkrankung der Hirnrinde. Allg Zeits Psychiatry Psych Y Gerichtl Med. 1907;64:146–148
5. Hebert LE, Scherr PA, Bienias JL, Bennett DA, Evans DA. Alzheimer disease in the US population: prevalence estimates using the 2000 census. Arch Neurol. 2003;60:1119–1122
6. O'Brien JA, Caro JJ. Alzheimer's disease and other dementia in nursing homes: levels of management and cost. Int Psychogeriatr. 2001;13:347–358
7. Stevens T, Livingston G, Kitchen G, Manela M, Walker Z, Katona C. Islington study of dementia subtypes in the community. Br J Psychiatry. 2002;180:270–276

8. Montine TJ, Phelps CH, Beach TG, Bigio EH, Cairns NJ, Dickson DW, Duyckaerts C, Frosch MP, Masliah E, Mirra SS, Nelson PT, Schneider JA, Thal DR, Trojanowski JQ, Vinters H V., Hyman BT. National institute on aging-Alzheimer's association guidelines for the neuropathologic assessment of Alzheimer's disease: A practical approach. Acta Neuropathol. 2012;123:1–11
9. Zhang Y, Thompson R, Zhang H, Xu H. APP processing in Alzheimer's disease. Mol Brain. 2011;4:3
10. Pryor EN, Moss MA, Hestekin CN. Unraveling the early events of amyloid-β protein (Aβ) aggregation: Techniques for the determination of Aβ aggregate size. Int J Mol Sci. 2012;13:3038–3072
11. Pike CJ, Overman MJ, Cotman CW. Amino-terminal deletions enhance aggregation of beta-amyloid peptides in vitro. J Biol Chem. 1995;270:23895–23898
12. Hardy J, Selkoe DJ. The amyloid hypothesis of Alzheimer's disease: progress and problems on the road to therapeutics. Science. 2002;297:353–356
13. Barten DM, Albright CF. Therapeutic strategies for Alzheimer's disease. Mol Neurobiol. 2008;37:171–186
14. Pey AL, Ying M, Cremades N, Velazquez-Campoy A, Scherer T, Thöny B, Sancho J, Martinez A. Identification of pharmacological chaperones as potential therapeutic agents to treat phenylketonuria. J Clin Invest. 2008;118:2858–2867
15. Cremades N, Velázquez-Campoy A, Martínez-Júlvez M, Neira JL, Pérez-Dorado I, Hermoso J, Jiménez P, Lanas A, Hoffman PS, Sancho J. Discovery of specific flavodoxin inhibitors as potential therapeutic agents against Helicobacter pylori infection. ACS Chem Biol. 2009;4:928–938
16. López LC, Dos-Reis S, Espargaró A, Carrodeguas JA, Maddelein ML, Ventura S, Sancho J. Discovery of novel inhibitors of amyloid beta-peptide 1-42 aggregation. J Med Chem. 2012;55:9521–9530
17. Laurents D V., Pantoja-Uceda D, López LC, Carrodeguas JA, Mompeán M, Jiménez MÁ, Sancho J. DMSO affects Aβ1–40's conformation and interactions with aggregation inhibitors as revealed by NMR. Rsc Adv. 2015;5:69761–69764
18. LeVine H. Thioflavine T interaction with synthetic Alzheimer's disease beta-amyloid peptides: detection of amyloid aggregation in solution. Protein Sci. 1993;2:404–410
19. Robbins KJ, Liu G, Selmani V, Lazo ND. Conformational analysis of thioflavin T bound to the surface of amyloid fibrils. Langmuir. 2012;28:16490–16495
20. Alteri CJ, Xicohténcatl-Cortes J, Hess S, Caballero-Olín G, Girón JA, Friedman RL. Mycobacterium tuberculosis produces pili during human infection. Proc Natl Acad Sci U S A. 2007;104:5145–5150
21. Taglialegna A, Lasa I, Valle J. Amyloid structures as biofilm matrix scaffolds. J Bacteriol. 2016;198:2579–2588
22. Schwartz K, Syed AK, Stephenson RE, Rickard AH, Boles BR. Functional amyloids composed of phenol soluble modulins stabilize Staphylococcus aureus biofilms. PLoS Pathog. 2012;8:e1002744
23. Marinelli P, Pallares I, Navarro S, Ventura S. Dissecting the contribution of Staphylococcus aureus α-phenol-soluble modulins to biofilm amyloid structure. Sci Rep. 2016;6:34552
24. El-Ahl A-AS, Ismail MA, Amer FA. Synthesis and Transformations of 2-Substituted Tetrahydro-4H-benzo[4,5]thieno[2,3-d][1,3]oxazines and 2,3-Disubstituted Hexahydrobenzo[4,5]thieno[2,3-d]pyrimidines. Phosphorus, Sulfur Silicon Relat Elem. 2003;178:245–259

25. Parra EJ, Rius FX, Blondeau P. A potassium sensor based on non-covalent functionalization of multi-walled carbon nanotubes. Analyst. 2013;138:2698–2703
26. Briel D, Rybak A, Kronbach C, Unverferth K. Substituted 2-Aminothiopen-derivatives: A potential new class of GluR6-Antagonists. Eur J Med Chem. 2010;45:69–77
27. Andersen HS, Olsen OH, Iversen LF, Sørensen ALP, Mortensen SB, Christensen MS, Branner S, Hansen TK, Lau JF, Jeppesen L, Moran EJ, Su J, Bakir F, Judge L, Shahbaz M, Collins T, Vo T, Newman MJ, Ripka WC, Møller NPH. Discovery and SAR of a novel selective and orally bioavailable nonpeptide classical competitive inhibitor class of protein-tyrosine phosphatase 1B. J Med Chem. 2002;45:4443–4459
28. Comito RJ, Finelli FG, Macmillan DWC. Enantioselective intramolecular aldehyde α-alkylation with simple olefins: Direct access to homo-ene products. J Am Chem Soc. 2013;135:9358–9361
29. Stocks PA, Bray PG, Barton VE, Al-Helal M, Jones M, Araujo NC, Gibbons P, Ward SA, Hughes RH, Biagini GA, Davies J, Amewu R, Mercer AE, Ellis G, O'Neill PM. Evidence for a common non-heme chelatable-iron-dependent activation mechanism for semisynthetic and synthetic endoperoxide antimalarial drugs. Angew Chemie - Int Ed. 2007;46:6278–6283
30. Sabnis RW, Rangnekar DW, Sonawane N. 2-aminothiophenes by the Gewald reaction. J Heterocycl Chem. 1999;36:333–345
31. Alexander M, Dalgleish DG. Dynamic light scattering techniques and their applications in food science. Food Biophys. 2006;1:2–13
32. Gao Z, Hao Y, Zheng M, Chen Y. A fluorescent dye with large Stokes shift and high stability: synthesis and application to live cell imaging. RSC Adv. 2017;7:7604–7609
33. Lindberg DJ, Wranne MS, Gilbert Gatty M, Westerlund F, Esbjörner EK. Steady-state and time-resolved Thioflavin-T fluorescence can report on morphological differences in amyloid fibrils formed by Aβ(1-40) and Aβ(1-42). Biochem Biophys Res Commun. 2015;458:418–423
34. Howie AJ, Brewer DB. Optical properties of amyloid stained by Congo red: History and mechanisms. Micron. 2009;40:285–301
35. Hackl E V., Darkwah J, Smith G, Ermolina I. Effect of acidic and basic pH on Thioflavin T absorbance and fluorescence. Eur Biophys J. 2015;44:249–261
36. Tehrani Bagha AR, Bahrami H, Movassagh B, Arami M, Menger FM. Interactions of gemini cationic surfactants with anionic azo dyes and their inhibited effects on dyeability of cotton fabric. Dye Pigment. 2007;72:331–338